# Nano-$WO_3$ film modified macro-porous silicon (MPS) gas sensor*

Sun Peng(孙鹏)†, Hu Ming(胡明), Li Mingda(李明达), and Ma Shuangyun(马双云)

School of Electronic and Information Engineering, Tianjin University, Tianjin 300072, China

**Abstract:** We prepared macro-porous silicon (MPS) by electrochemical corrosion in a double-tank cell on the surface of single-crystalline P-type silicon. Then, nano-$WO_3$ films were deposited on MPS layers by DC facing target reactive magnetron sputtering. The morphologies of the MPS and $WO_3$/MPS samples were investigated by using a field emission scanning electron microscope. The crystallization of $WO_3$ and the valence of the W in the $WO_3$/MPS sample were characterized by X-ray diffraction and X-ray photoelectron spectroscopy, respectively. The gas sensing properties of MPS and $WO_3$/MPS gas sensors were thoroughly measured at room temperature. It can be concluded that: the $WO_3$/MPS gas sensor shows the gas sensing properties of a P-type semiconductor gas sensor. The $WO_3$/MPS gas sensor exhibits good recovery characteristics and repeatability to 1 ppm $NO_2$. The addition of $WO_3$ can enhance the sensitivity of MPS to $NO_2$. The long-term stability of a $WO_3$/MPS gas sensor is better than that of an MPS gas sensor. The sensitivity of the $WO_3$/MPS gas sensor to $NO_2$ is higher than that to $NH_3$ and $C_2H_5OH$. The selectivity of the MPS to $NO_2$ is modified by deposited nano-$WO_3$ film.

**Key words:** MPS; $WO_3$/MPS gas sensor; gas sensing properties; room temperature
**DOI:** 10.1088/1674-4926/33/5/054012 **PACC:** 8160C; 8280T

## 1. Introduction

With more and more contaminated gas emissions from industry and daily life, novel high-performance and low-power gas sensors have attracted increasing attention. Porous silicon (PS), which has high specific area can be used as an alternative material for gas sensors operated at room temperature[1−4]. Conductivity variation of this material is the easiest way to realize a gas sensor for gas detection. It is easy to integrate PS with current CMOS/MEMS technologies[5−8] thereby reducing the cost of devices, which is important for its practical application.

The pore diameter of PS can be controlled from tens of nanometers[9] to a few micrometers[10, 11] by changing formation parameters. Macro-porous silicon (MPS) is a kind of PS that has an average pore diameter of more than 50 nm. MPS has recently attracted the attention of the scientific community for its various applications in photonic devices[12], micro-fuel cell electrodes[13], supercapacitors[14], biosensors[15] and gas sensors[16]. An MPS layer has low porosity, which results in low sensitivity when used as a gas sensor. In recent years, some researchers have deposited the modified layer on the MPS surface to improve its gas sensing properties. Kanungo *et al.*[17] produced a reliable and stable MPS hydrogen sensor working at an elevated temperature by depositing the ZnO thin film on MPS. Ozdemir and Gole[18] deposited metal oxide coatings on the MPS surface and improved the sensitivity of MPS to $PH_3$. Galstyan *et al.*[19] developed a high sensitivity and stability hydrogen gas sensor made of MPS covered with thin metal oxide film. However, there are a few articles reporting on the improvement of the gas sensing properties of MPS to $NO_2$.

In this work, $WO_3$ modified layers were deposited on MPS. We investigated the gas sensing properties of MPS and $WO_3$/MPS gas sensors for detecting different concentrations of $NO_2$ at room temperature. Our study indicates that the addition of $WO_3$ can enhance the sensitivity, improve the long-term stability and modify the selectivity of the MPS to $NO_2$.

## 2. Experimental details

MPS layers were formed by electrochemical corrosion of (100)-oriented monocrystalline P-type silicon wafers with 10–15 Ω·cm resistivity and 400 ±10 $\mu$m thickness in a double-tank cell. The electrolyte consisted of 99.5 wt.% N, N-Dimethylformamide (DMF) and 40 wt.% hydrofluoric acid in a volume ratio of 2 : 1. The etching current density was 100 mA/cm$^2$. The etching time for all samples was 5 min. Then the nano-$WO_3$ films were deposited on MPS layers using the dc reactive magnetron sputtering method. The deposited thin films were annealed at a temperature of 450 ℃ for 4 h in air. Pt electrodes were deposited on the top of the MPS and $WO_3$/MPS to form MPS and $WO_3$/MPS gas sensors. The sputtering conditions of different metals are shown in Table 1. The schematic diagrams of the MPS and $WO_3$/MPS gas sensors are shown in Fig. 1.

The surface and cross-section images of MPS and $WO_3$/MPS samples were obtained by using a field emission scanning electron microscope (FESEM, Nanosem 430). The crystallization of $WO_3$ and the valence of the W in the $WO_3$/MPS sample were respectively characterized by X-ray diffraction (XRD, D/MAX 2500) and X-ray photoelectron spectroscopy (XPS, PHI-1600). Gas sensing characteristics of MPS and $WO_3$/MPS gas sensors were measured at room tem-

* Project supported by the National Natural Science Foundation of China (No. 60771019) and the Tianjin Key Research Program of Application Foundation and Advanced Technology, China (No. 11JCZDJC15300).
† Corresponding author. Email: sunpengtju@163.com
Received 11 October 2011, revised manuscript received 23 December 2011 

Table 1. Preparation conditions of different metals.

| Sputtering target | Sputtering pressure (Pa) | Sputtering gas mixture ratio | Sputtering time (min) | Sputtering power (W) |
|---|---|---|---|---|
| W | 1 | $Ar : O_2 = 30 : 20$ | 30 | 100 |
| Pt | 2 | Ar | 10 | 90 |

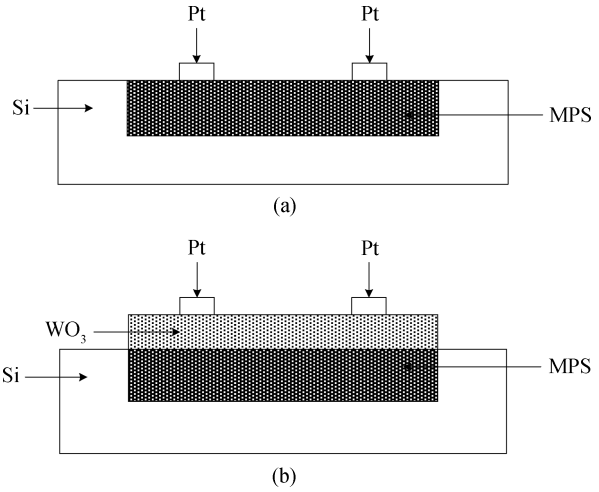


Fig. 1. Schematic diagrams of the (a) MPS and (b) $WO_3$/MPS gas sensors.

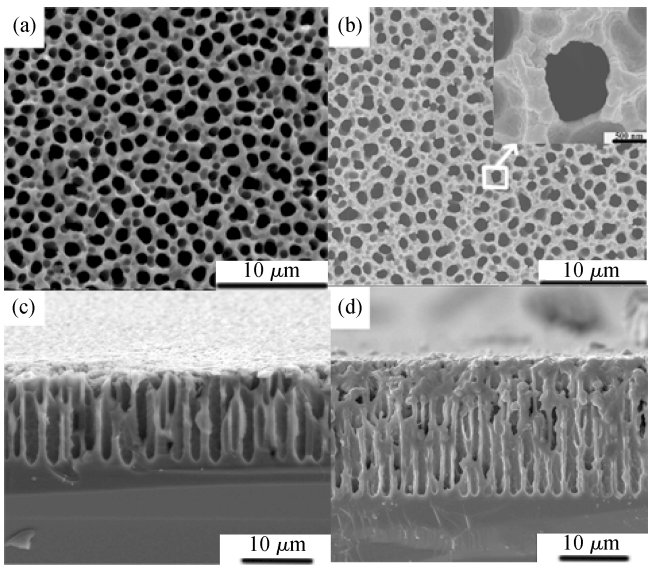


Fig. 2. SEM images of the (a, c) MPS and (b, d) $WO_3$/MPS. (a, b) Surface morphology. (c, d) Cross-section morphology.

perature. The sensors were placed in a 30 liter test chamber. The testing gas was directly injected into the chamber to get the desired concentration. The sensor sensitivity ($S$) is defined as $R_g/R_a$ or $R_a/R_g$ for reducing or oxidizing gases, respectively, where $R_a$ is the resistance value in the presence of the ambient atmosphere and $R_g$ is the resistance value in the presence of the measured species.

## 3. Results and discussion

### 3.1. Morphology of MPS and $WO_3$/MPS samples

Figures 2(a) and 2(b) show the surface morphology images of the MPS and $WO_3$/MPS samples with a hole-shaped frame.

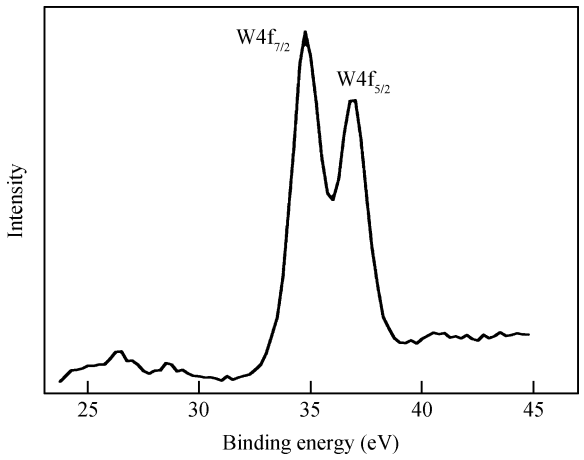


Fig. 3. Binding energy of W4f $WO_3$/MPS sample.

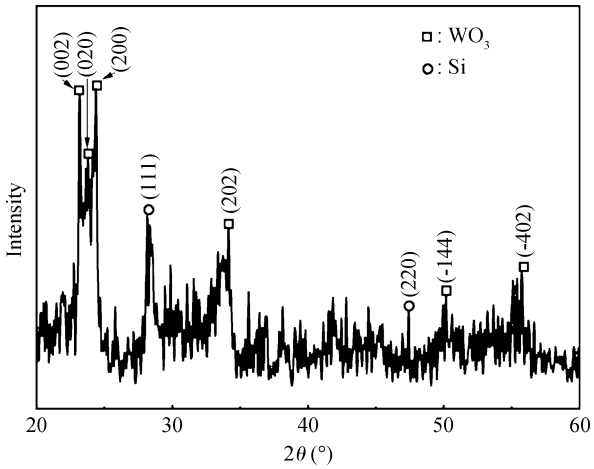


Fig. 4. XRD analysis of $WO_3$/MPS sample.

It can be concluded that the average pore size of the MPS is 1.5 $\mu$m and $WO_3$ nano-particles form a semi-continuous thin film on the surface of MPS layer. Figures 2(c) and 2(d) present the cross-section morphology images of the MPS and $WO_3$/MPS samples. The typical pore depth is 12 $\mu$m and the micropores are cylindrical in shape with a conical termination at the c-Si interface of the anodized wafer (Fig. 2(c)). There is a nano-$WO_3$ film on the surface of the MPS (Fig. 2(d)). The structure of the MPS is not destroyed by the deposited nano-$WO_3$ film.

### 3.2. X-ray photoelectron spectroscopy analysis

Figure 3 shows the binding energy of W4f of the $WO_3$/MPS sample. The binding energy of $W4f_{7/2}$ and $W4f_{5/2}$ are determined to be 34.8 and 37.0 eV, respectively, which do not agree well with values for $W^{6+}$ from Ref. [20]. The spectrum shifts towards a lower binding energy; this may be caused

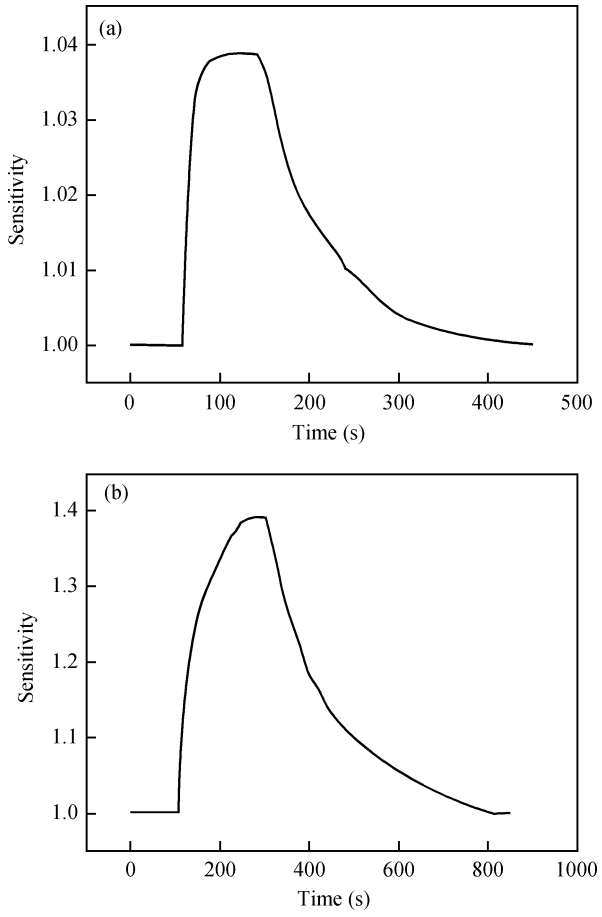


Fig. 5. Responses of (a) MPS and (b) $WO_3$/MPS gas sensors to 1 ppm $NO_2$ at room temperature.

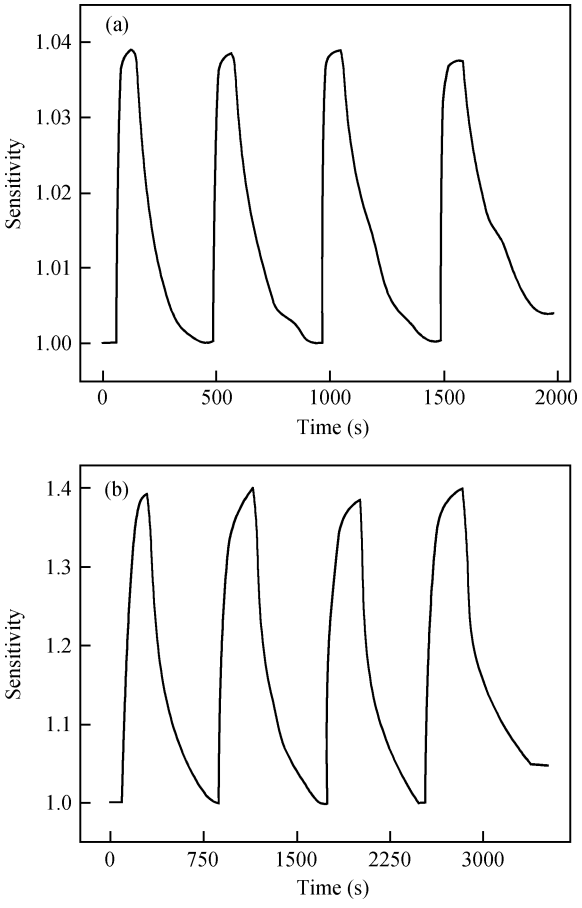


Fig. 6. Dynamic responses of (a) MPS and (b) $WO_3$/MPS gas sensors to 1 ppm $NO_2$ at room temperature.

by the contribution from $W^{5+}$ or $W^{4+}$ states, resulting from oxygen vacancies in the film. It was reported that these states could play important roles in the sensor's performance[21].

### 3.3. X-ray diffraction analysis

Figure 4 shows the XRD pattern of the $WO_3$/MPS sample. It can be seen that $WO_3$ exhibits a triclinic phase (PDF20-1323). There are some diffraction peaks at (002), (020), (200), (022), (−114) and (−402) crystal faces. The strongest peak lies at $2\theta = 24.4°$. However, the noise of the XRD pattern is rather high due to the thin thickness and rough surface of the nano-$WO_3$ film.

### 3.4. Gas sensing properties of MPS and $WO_3$/MPS gas sensors

Figure 5 shows the responses of the MPS and $WO_3$/MPS gas sensors to 1 ppm $NO_2$ at room temperature. The detection sensitivity in the oxidizing gas is greater than 1. It can be concluded that the resistance values of sensors decrease rapidly when $NO_2$ is introduced into the measurement chamber. Upon exposing the sensors to air by opening the chamber, the resistance values of the sensors gradually increase to the initial values. The sensors have shown P-type semiconductor gas sensor behavior for oxidizing gas. The sensitivity of the $WO_3$/MPS gas sensor is much higher than that of the MPS gas sensor. The $WO_3$/MPS gas sensor shows good response-recovery characteristics to 1 ppm $NO_2$. But the response time and recovery time of the $WO_3$/MPS gas sensor are longer than those of MPS gas sensor since the nano-$WO_3$ film covers the MPS surface which inhibits the diffusion of the gas.

Figure 6 presents the dynamic responses of MPS and $WO_3$/MPS gas sensors to 1 ppm $NO_2$ at room temperature. The average sensitivity is 1.04 and 1.40 for MPS gas sensor and $WO_3$/MPS gas sensor, respectively. The overall variations in sensor sensitivity, response time and recovery time are very small for both gas sensors, which indicates good repeatability of the MPS and $WO_3$/MPS gas sensors to 1 ppm $NO_2$. Moreover, after four times repeating, the resistance values of the MPS and $WO_3$/MPS gas sensors can almost recover to their initial values, which shows good reproducibility to 1 ppm $NO_2$.

Figure 7 shows the responses of MPS and $WO_3$/MPS gas sensors to different $NO_2$ concentrations at room temperature. From this figure, it can be seen that the sensitivity values of the $WO_3$/MPS gas sensor upon exposure to 1, 10, 25 and 50 ppm $NO_2$ are 1.40, 5.01, 9.01 and 14.4, while those of the MPS gas sensor are 1.04, 1.18, 1.25 and 1.34, respectively. All of the sensitivity values of the gas sensors increase with the mounting up of the $NO_2$ concentration. It also can be seen that the $WO_3$/MPS gas sensor has higher sensitivity than that of the MPS gas sensor in each $NO_2$ gas concentration.

As $NO_2$ is an oxidizing gas, it causes local and partial oxidation of the MPS surface, which causes the increase of defect

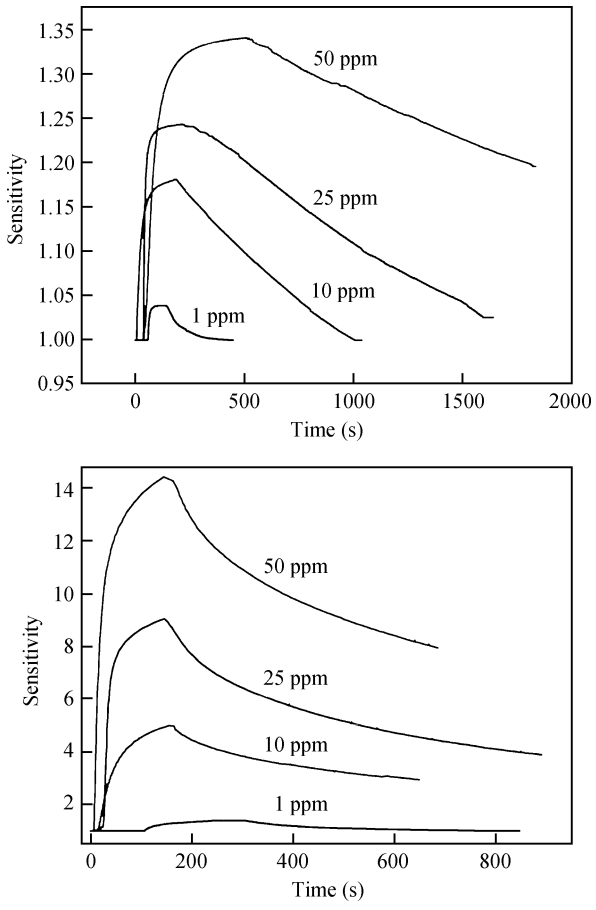


Fig. 7. Responses of (a) MPS and (b) $WO_3$/MPS gas sensors to different $NO_2$ concentrations at room temperature.

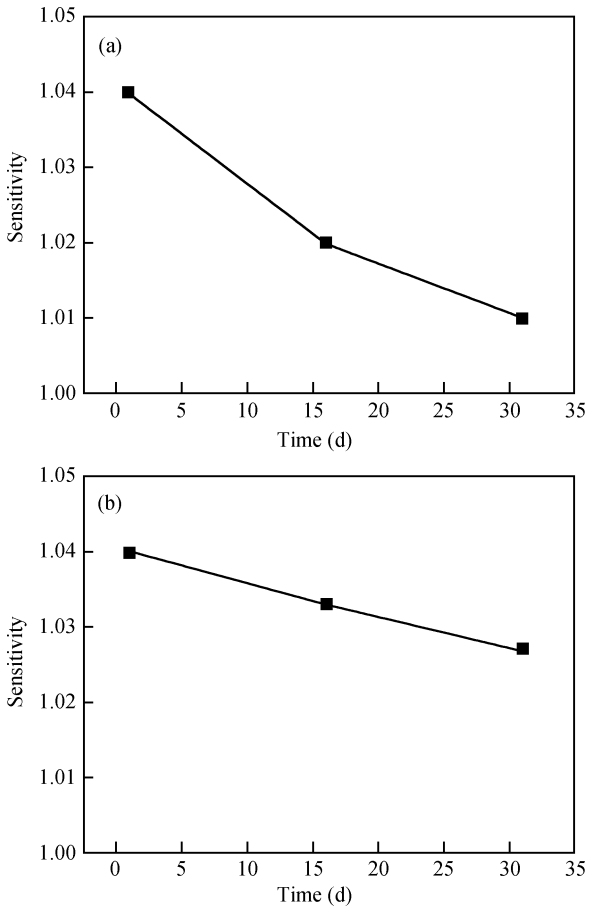


Fig. 8. Sensitivity of (a) MPS and (b) $WO_3$/MPS gas sensors to 1 ppm $NO_2$ for different storage days.

density. These defects play the role of electron traps, into which electrons relax[22, 23]. Therefore, it seems that the electron traps created by partial oxidation of MPS in the presence of $NO_2$ are responsible for the increase of free charge carriers in P-type MPS. Since $WO_3$ behaves as an n-type semiconductor gas sensor which is controlled by the surface conductance[24, 25], the hetero-structure (n-$WO_3$/p-MPS) is formed at the interface between $WO_3$ and MPS. In the hetero-structure, there exists a depletion layer and associated potential barrier. The concentration of free carriers in the MPS increases when MPS adsorbs $NO_2$. The width of the depletion layer gets smaller and the potential barrier gets lower. It may bring in additional increasing part of the current. This change may explain the improvement in responsiveness shown by $WO_3$/MPS gas sensor. Moreover, $WO_3$ is a good gas sensing material for $NO_2$. It has good selectivity to $NO_2$[26, 27]. In the combined structure, the improvement of gas sensing properties observed may be attributed to the effects of $WO_3$ as a catalyst on the surface of the MPS.

Although the sensitivity of the $WO_3$/MPS gas sensor to $NO_2$ is higher than that of MPS gas sensor, the baseline shifting of the gas sensor is more obviously for $WO_3$/MPS gas sensor, especially at high concentrations (above 10 ppm). The nano-$WO_3$ which inhibits the diffusion of the gas results in poor recover characteristic at relative high $NO_2$ concentrations.

The long-term stability of the sensors was investigated by testing the sensitivity to 1 ppm $NO_2$ for different storage days. The results are shown in Fig. 8. On one hand the sensitivity of the sensors shows evident changes over 30 days storage which indicates that the long-term stability of the gas sensors is not very good. On the other hand, it also can be seen that the sensitivity of the $WO_3$/MPS gas sensor changes more slowly than that of the MPS gas sensor. The nano-$WO_3$ may make surface passivation of the MPS, which causes a better long-term stability of $WO_3$/MPS gas sensor.

To examine the selectivity of MPS and $WO_3$/MPS gas sensors, the sensors have been tested to other two gases (50 ppm). The results are shown in Fig. 9, revealing that the $WO_3$/MPS gas sensor exhibits the best sensitivity to $NO_2$ with a value of 14.4, while MPS gas sensor exhibits the best sensitivity to $NH_3$ with a value of 4.2. The selectivity of the MPS to $NO_2$ is modified by deposited nano-$WO_3$ film.

## 4. Conclusions

MPS layers were obtained by electrochemical dissolution in a double-tank cell on the surface of the monocrystalline P-type silicon. The MPS layer is with a depth of 12 $\mu$m and a normal size of the pore about 1.5 $\mu$m. The nano-$WO_3$ films prepared by DC reactive magnetron sputtering were deposited on the MPS layer. Nano-$WO_3$ film exhibits triclinic phase. XPS test shows that the valence of the W is consisted of $W^{6+}$, $W^{5+}$ and $W^{4+}$ states.

The gas sensing properties measurements indicate that low concentration of 1 ppm $NO_2$ can be detected even when the

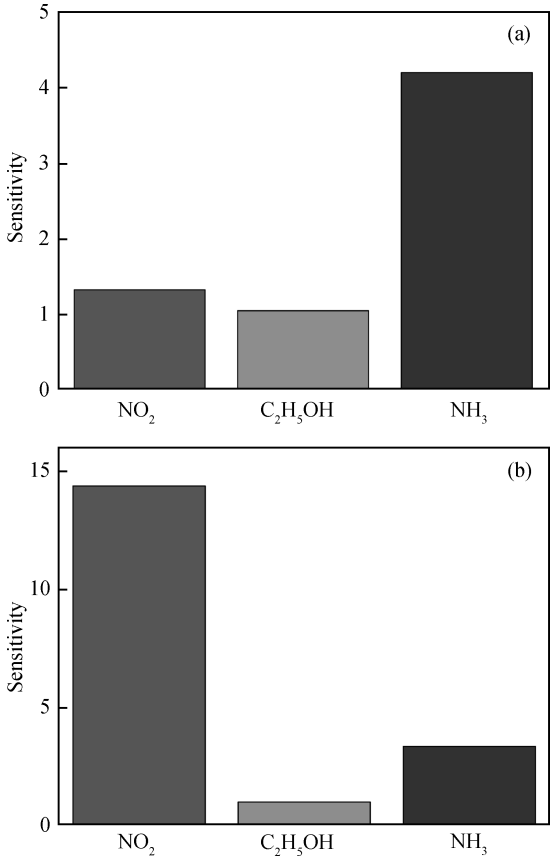


Fig. 9. Sensitivity of (a) MPS and (b) $WO_3$/MPS gas sensors to 50 ppm various gases at room temperature.

$WO_3$/MPS sensor is operated at room temperature. The sensitivity of the $WO_3$/MPS gas sensor is much higher than that of MPS gas sensor in each $NO_2$ concentration. The long-term stability and selectivity are also improved.

## References

[1] Kanungo J, Saha H, Basu S. Effect of porosity on the performance of surface modified porous silicon hydrogen sensors. Sensors and Actuators B: Chemical, 2010, 147(1): 145

[2] Jalkanen T, Salonen J, Torres-Costa V, et al. Structural considerations on multistopband mesoporous silicon rugate filters prepared for gas sensing purposes. Opt Express, 2011, 19(14): 13291

[3] Kim H J, Kim Y Y, Lee K W. Multiparametric sensor based on DBR porous silicon for detection of ethanol gas. Current Appl Phys, 2010, 10(1): 181

[4] Ozdemir S, Gole J L. The potential of porous silicon gas sensors. Current Opinion in Solid State and Materials Science, 2007, 11(5/6): 92

[5] Barillaro G, Bruschi P, Lazzerini G M, et al. Validation of the compatibility between a porous silicon-based gas sensor. IEEE Technology and Standard Microelectronic Process Sensors Journal, 2010, 10(4): 893

[6] Barillaro G, Nannini A, Pieri F. APSFET: a new, porous silicon-based gas sensing device. Sensors and Actuators B: Chemical, 2003, 93(1–3): 263

[7] Zhou Yi, Yang Li, Zhang Guoyan, et al. Fabrication of a porous silicon new substrate for a high *Q* radio frequency integrated inductor. Chinese Journal of Semiconductors, 2005, 26(6): 1182

[8] Zhou Jun, Wang Xiaohong, Yao Pengjun, et al. Analysis and design of an accelerometer fabricated with porous silicon as sacrificial layer. Chinese Journal of Semiconductors, 2003, 24(7): 687

[9] Fang Zhenqian, Hu Ming, Zhang Wei, et al. Mechanical properties of porous silicon by depth-sensing nanoindentation techniques. Thin Solid Films, 2009, 517(9): 2930

[10] Mathwig K, Geilhufe M, Müller F, et al. Bias-assisted KOH etching of macroporous silicon membranes. J Micromechan Microeng, 2011, 21(3): 035015

[11] Maji S, Das R D, Jana M, et al. Formation of ohmic contact by pre-annealing of shallow nanopores in macroporous silicon and its characterization. Solid-State Electron, 2010, 54(5): 568

[12] Yang Hongta, Jiang Peng. Macroporous photonic crystal-based vapor detectors created by doctor blade coating. Appl Phys Lett, 2011, 98: 011104

[13] Nikulin A Y, Pelliccia D, Starkov V V, et al. Columnar structure in porous silicon: influence of etching time on pore dynamics and ordering. J Appl Phys, 2011, 109(7): 076106

[14] Sancho A, Arizti F, Gracia F J. Porous silicon for the development of capacitive microstructures. Microelectron Eng, 2009, 86(11): 2144

[15] Steinhauer C, Ressine A, Marko-Varga G, et al. Biocompatibility of surfaces for antibody microarrays: design of macroporous silicon substrates. Analytical Biochemistry, 2005, 341(2): 204

[16] Wanga Y, Parka S, Yeowa J T W, et al. A capacitive humidity sensor based on ordered macroporous silicon with thin film surface coating. Sensors and Actuators B: Chemical, 2010, 149(1): 136

[17] Kanungo J, Saha H, Basu S. Pd sensitized porous silicon hydrogen sensor—influence of ZnO thin film. Sensors and Actuators B: Chemical, 2010, 147(1): 128

[18] Ozdemir S, Gole J L. A phosphine detection matrix using nanostructure modified porous silicon gas sensors. Sensors and Actuators B: Chemical, 2010, 151(1): 274

[19] Galstyan V E, Martirosyan K S, Aroutiounian V M, et al. Investigations of hydrogen sensors made of porous silicon. Thin Solid Films, 2008, 517(1): 239

[20] Stankova M, Vilanova X, Llobet E, et al. Influence of the annealing and operating temperatures on the gas-sensing properties of RF sputtered $WO_3$ thin-film sensors. Sensors and Actuators B: Chemical, 2005, 111/112(2): 271

[21] Ottaviano L, Bussolotti F, Lozzi L, et al. Core level and valence band investigation of $WO_3$ thin films with synchrotron radiation. Thin Solid Films, 2003, 436(1): 9

[22] Razi F, Rahimi F, Irajizad A. Fourier transform infrared spectroscopy and scanning tunneling spectroscopy of porous silicon in the presence of methanol. Sensors and Actuators B: Chemical, 2008, 132(1): 40

[23] Salonen J, Lehto V P, Laine E. The room temperature oxidation of porous silicon. Appl Surf Sci, 1997, 2(3/4): 191

[24] Sun Fengyun, Hu Ming, Sun Peng, et al. $NH_3$ sensing characteristics of nano-$WO_3$ thin films deposited on porous silicon. J Nanosci Nanotechnol, 2010, 10(11): 7739

[25] Qin Yuxiang, Hu Ming, Zhang Jie. Microstructure characterization and $NO_2$-sensing properties of tungsten oxide nanostructures. Sensors and Actuators B: Chemical, 2010, 150(1): 339

[26] Qin Yuxiang, Shen Wanjiang, Li Xiao, et al. Effect of annealing on microstructure and $NO_2$-sensing properties of tungsten oxide nanowires synthesized by solvothermal method. Sensors and Actuators B: Chemical, 2011, 155(2): 646

[27] Kim S J, Hwang I S, Choi J K, et al. Gas sensing characteristics of $WO_3$ nanoplates prepared by acidification method. Thin Solid Films, 2011, 519(6): 2020